Journal of Materials Processing Technology xxx (2010) xxx–xxx

Contents lists available at ScienceDirect

Journal of Materials Processing Technology

journal homepage: www.elsevier.com/locate/jmatprotec

# Database for real-time loading path prediction for tube hydroforming using multidimensional cubic spline interpolation

Angshuman Ghosh, Karan Deshmukh, Gracious Ngaile*

*Department of Mechanical & Aerospace Engineering, North Carolina State University, Box 7910, Raleigh, NC 27695, USA*

ARTICLE INFO

*Article history:*
Received 8 December 2009
Received in revised form 4 September 2010
Accepted 17 September 2010
Available online xxx

*Keywords:*
Tube hydroforming
Loading path
Interpolation

ABSTRACT

Tube hydroforming (THF) is a metal-forming process that uses a pressurized fluid in place of a hard tool to plastically deform a given tube into a desired shape. In addition to the internal pressure, the tube material is fed axially toward the die cavity. This process has various applications in the automotive, aerospace, and bicycle industries. Accurate coordination of the fluid pressure and axial feed, collectively referred to as a loading path, is critical to THF. Workable loading paths are currently determined by trial and error, which can be time consuming.

This study discusses an innovative technique for developing an interactive, real-time database that would be able to predict loading paths for many THF components and hence reduce the computational time required. By classifying most of the commercial THF parts into families, parameters such as material properties, part geometry, and tribological factors were simulated by category and stored in the database. Multidimensional cubic spline interpolation was implemented to enable an end user to request from the database a loading path for a wide range of conditions. Test results from the database for different THF families were shown to approximate the simulated results. In addition to reducing the computation time, the use of interpolation techniques eliminates the need for carrying out multiple simulations for similar THF parts.



## 1. Introduction

Hydroforming has found significant industrial utility in the present decade, although research on tube hydroforming started in the 1940s (Koc and Altan, 2001). Automotive parts that are typically produced using this process include exhaust manifolds, chassis, engine cradles, and radiator frames. Hydroforming allows weight reduction without compromising strength, which is of great significance in the automotive and aerospace industries. For example, conventional fabrication of a chassis involves welding several parts together, whereas hydroforming can manufacture a chassis in a single step, thus reducing weight and secondary operations.

Tube hydroforming (THF) is a metal-forming process in which a tube is plastically expanded into a die cavity by the simultaneous action of fluid pressure and axial material feed, such that the tube takes the shape of the die cavity. Success of THF depends on various process and material parameters. The two most important process parameters are internal pressure (Fig. 1a) given to the tube and axial material feed (Fig. 1b) applied to the ends of the tube. A graphical representation of the two parameters is called a loading path (Fig. 1c). Loading path depends on process conditions and materials and is independent of process time. Also, loading path has to be in a particular process window for the part to be successfully formed, as shown in Fig. 1c. Inaccurate loading path will lead to part failures such as wrinkling, bursting, or buckling. The details on the modes of failure and mathematical models for failure predictions are given by Dohmann and Hartl (1997) and Xia (2001), respectively.

Prediction of the proper loading path for a particular set of process conditions is one of the biggest challenges in THF. Since this process is relatively new, much is not known. Previous attempts to predict loading paths have mostly involved trial-and-error. Reducing the computational time required for loading-path prediction would increase the utility of THF. The following are some of the attempts to develop a faster and more systematic approach to loading-path prediction:

*Trial and Error FEA Simulation approach*: One of the first improvements over trial-and-error was the use of FEA analysis, where iterative FE simulations are carried out until acceptable forming results are obtained. This process is still extremely inefficient and time consuming (Strano et al., 2004). To reduce the number of simulations, the minimum axial feed of the materials can be established by carrying out simulation without forced axial feeding, i.e.,

* Corresponding author.
*E-mail address:* gracious_ngaile@ncsu.edu (G. Ngaile).

0924-0136/$ – see front matter © 2010 Elsevier B.V. All rights reserved.
doi:10.1016/j.jmatprotec.2010.09.012

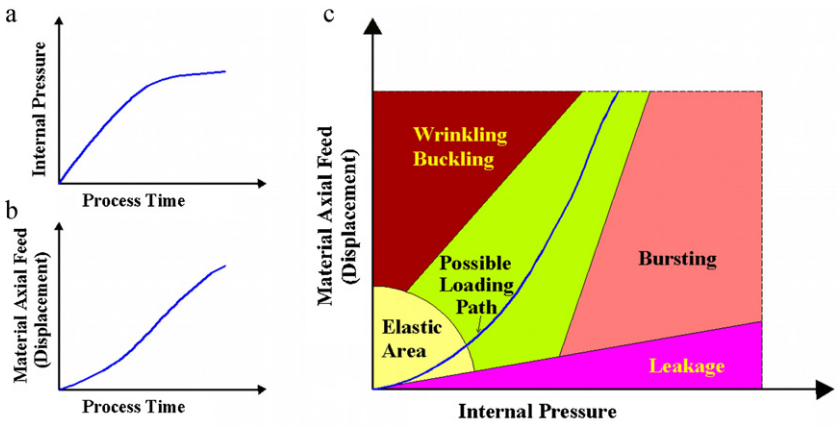


**Fig. 1.** Process window for THF process and loading path.

the axial feed obtained from this simulation is due to the action of internal pressure only. This technique is known as self-feeding and provides the initial loading path (Strano et al., 2004).

*Optimization approach*: This approach aims at optimizing local tube-wall thickness distribution by sensitivity analysis. Repeated simulations are carried out until an optimal loading path is obtained (Gelin and Labergere, 2002).

*Adaptive approach*: The adaptive method is faster than the above methods in that it determines the process-loading curve by running a single simulation. The method monitors the failure modes of wrinkling and bursting with the use of indicators inside the FEA simulation itself. This is done by defining failure indicators, namely, the wrinkle indicator and the bursting indicator (Nordlund, 1998). The control strategy identifies the wrinkle or bursting with the help of these indicators and gives feedback to the simulation, where changes are made to prevent failure

*Fuzzy Load Control method and Neural Network Analysis method*: Fuzzy Load Control (FLC) involves development of fuzzy logic rules based on previous knowledge of the THF process window (Ray and Mac Donald, 2004). Using these rules, failure indicators based on threshold for wrinkling and buckling, are decided. The simulation procedure differs from the adaptive approach such that here the failure indicators are decided based on fuzzy logic rules. Ray and Mac Donald (2004) used FLC to predict loading paths for T-shape THF. Lin and Kwan (2004) presented four-layer and five-layer abductive network models to predict the process parameters of THF for an acceptable T-shape product. They chose a material with a constant shear friction and varied the geometrical parameters of the die cavity and the internal pressure input to get a total of 75 sets of parameters. Then they obtained the training data by performing FEA simulation on those 75 sets using the commercial FEA simulation software DEFORM 3D.

All the methods discussed above expend considerable time in searching for a loading path that will result in a successful part. Moreover, most of those methods can only be used to obtain a loading path for a specific material and geometry, i.e., they must be rerun if the THF geometry or material has changed. This study proposes the development of a database that through interpolation could instantly provide continuous loading-path data for THF parts with different materials and geometries.

## 2. Objectives and approaches

The objectives of this study are to (a) develop a database containing loading-path data for forming numerous THF components with different materials, geometries, and tribological conditions and (b) establish a multidimensional interpolation scheme in conjunction with the FE-based simulation database that will facilitate determination of real-time continuous loading paths for THF parts. The approaches taken to achieve the above objectives are presented in the flowchart shown in Fig. 2.

## 3. Classifications of THF components

A thorough review on commercially available THF components was carried out in order to classify THF families for the database as shown in Fig. 3. However, the scope of this study is limited to the families that require both axial feed and internal pressure for forming. Hence seven families were selected for this study namely Bulge shape (B), Single Y shape (SY), Aligned Double Y shape (DY), Single T shape (ST), Aligned Double T shape (DT), Non Aligned Double T shape – opposite side (DTOS) and Non Aligned Double T shape – same side (DTSS). Fig. 4 shows schematics of the seven THF families.

## 4. Pressure curve generation and strategy

Pressure and material feed profiles are the two components that build up the loading paths for THF. This section will focus on pressure curve generation and the next section will be devoted on material feed curves. The strategy taken in generating the loading paths was to obtain a generic pattern for the pressure profile. That is, the pressure curves which will have the sample pattern for all THF families. Having a generic pressure profile will lead to a robust interpolation scheme as compared to using different patterns of pressure profiles for different THF families. It should be noted that the loading path for THF is composed of the pressure loading and material feed profiles as shown in Fig. 1a and b. Theoretically, infinite routes are possible to obtain the loading path (material feed vs. pressure) shown in Fig. 1c. For example, three different scenarios to obtain the same loading path shown in Fig. 1c can be examined. In scenario A, one could fix material feed profile and vary the pressure profile, whereas in scenario B, pressure profile could be fixed and the material feed profile could be varied. In scenario C, both pressure and material feed profiles could be varied. The common boundary conditions for all three scenarios are (a) at the end of the process a certain maximum forming pressure will be needed to ensure that the desired corner radii are formed and (b) at the end of the process a certain amount of material should have been fed to the die cavity to ensure that the part is successfully hydroformed. In this study scenario B was adopted, where the pattern of the pressure profile is fixed for all THF families.

The unit pressure curve shown in Fig. 5 was adopted for this study. The specific profile in Fig. 5 shows various stages in the THF

Please cite this article in press as: Ghosh, A., et al., Database for real-time loading path prediction for tube hydroforming using multidimensional cubic spline interpolation. J. Mater. Process. Tech. (2010), doi:10.1016/j.jmatprotec.2010.09.012

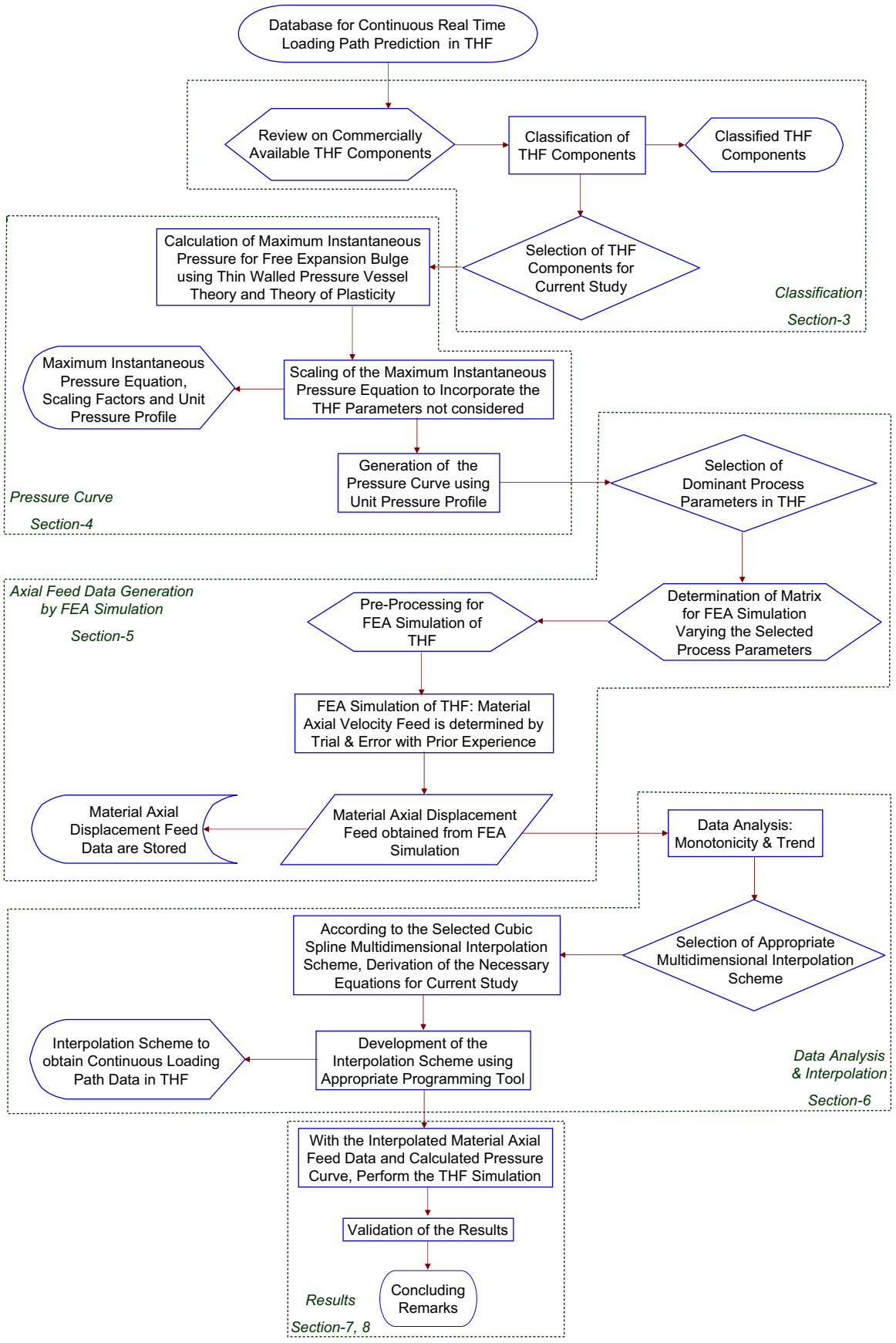


**Fig. 2.** Flowchart showing the approaches taken in this study.

Please cite this article in press as: Ghosh, A., et al., Database for real-time loading path prediction for tube hydroforming using multidimensional cubic spline interpolation. J. Mater. Process. Tech. (2010), doi:10.1016/j.jmatprotec.2010.09.012

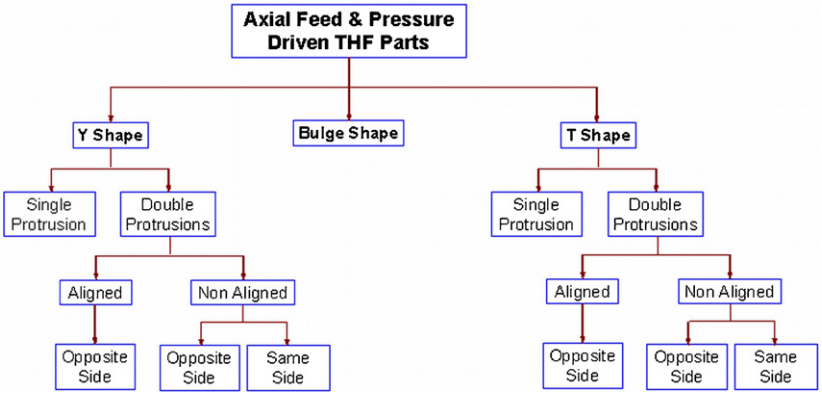


**Fig. 3.** Classification of axial feed and pressure driven THF components.

process. *Yielding*: This part of the curve should maintain a linearly increasing profile during yielding. *Expansion*: During this stage the gradient is reduced. This enhances more material feed compared to pressure. *Calibration*: During this stage, the pressure increases to its maximum value to fill the corners and radii.

This unit pressure profile would then be multiplied by the maximum pressure to obtain the actual pressure curve for a specific THF geometry. Using a third degree polynomial shown in Eq. (1), unit pressure profile is estimated for a unit process time, where $T$ denotes the time. It should be noted that a different unit pressure profile could have been adopted.

$$P_u = 1.67T^3 - 4T^2 + 3.33T \tag{1}$$

### 4.1. Determination of the maximum instantaneous pressure

The prediction of instantaneous pressure for bulge family is proposed based on the assumptions that the tube is thin and obeys membrane theory and the maximum thinning before fracture is 30%. Fig. 6 shows a bulge tube under internal instantaneous pressure ($P_i$) and material feed ($f$) supplied by the punches. The figure also shows an element of the bulge tube showing tangential stress ($\sigma_a$) and axial stress ($\sigma_b$). However the radial stress ($\sigma_r$) is assumed to be negligible compared to the other stresses.

The instantaneous pressure ($P_i$) at the instant of final forming for a thin cylindrical tube could be given by Eq. (2), where, $t_i$ is the minimum final instantaneous thickness of the tube at 30% thinning ($t_i = 0.7t_0$) in the expansion zone and $d_i$ is the maximum final instantaneous diameter in the expansion zone (Asnafi, 1999). Due to plane stress condition ($\sigma_r = 0$), the radial strain ($\varepsilon_r$) and tangential strain ($\varepsilon_a$) are defined by Eqs. (3) and (4) respectively. Using the Von Mises criteria, the effective stress and strain can be defined by Eqs. (5) and (6) respectively.

$$P_i = \frac{2\sigma_a t_i}{d} \tag{2}$$

$$\varepsilon_r = \ln\left(\frac{t_i}{t_0}\right) \tag{3}$$

$$\varepsilon_a = \ln\left(\frac{d_i - t_i}{d_0 - t_0}\right) \tag{4}$$

$$\bar{\varepsilon} = \frac{2}{\sqrt{3}}\varepsilon_a(1 + \beta + \beta^2)^{1/2} \tag{5}$$

$$\bar{\sigma} = (1 - \alpha + \alpha^2)^{1/2}\sigma_a \tag{6}$$

where $\alpha = \sigma_b/\sigma_a$ and $\beta = \varepsilon_b/\varepsilon_a$

$$\bar{\sigma} = K(\bar{\varepsilon})^n \tag{7}$$

By assuming that the material follows the power law given in Eq. (7) and relating Eqs. (2), (5), (6) and (7), an expression could be derived for instantaneous pressure ($P_i$) as a function of $K$, tube geometrical variables, stress and strain as shown in Eq. (8), where, $K$ is the material strength coefficient and $n$ is strain hardening coefficient. Since Eq. (8) gives the instantaneous pressure of the system at the final time step, this is the maximum instantaneous pressure ($P_f$) for the bulged tube.

$$P_i = \frac{2t_i}{d_i - t_i}\frac{K\left((2/\sqrt{3})(1 + \beta + \beta^2)^{1/2}.\varepsilon_a\right)^n}{(1 - \alpha + \alpha^2)^{1/2}} \tag{8}$$

In Eq. (8) $\beta$ and $\alpha$ need to be determined. Using the volume constancy given in Eq. (9), $\beta$ ($\beta = \varepsilon_b/\varepsilon_a$) could be expressed in terms of $\varepsilon_a$ and $\varepsilon_r$ as shown in Eq. (10). Using the relation of principal stresses, $\alpha$ could be obtained from Eqs. (11) and (12). By multiplying the maximum instantaneous pressure (Eq. (8)) by the unit pressure ($P_u$), Eq. (1), Eq. (13) can be obtained.

$$\varepsilon_a + \varepsilon_b + \varepsilon_r = 0 \tag{9}$$

$$\beta = -\left(\frac{\varepsilon_r}{\varepsilon_a} + 1\right) \tag{10}$$

$$\sigma_1 = \frac{\bar{\sigma}}{\bar{\varepsilon}}\left[\varepsilon_1 + \frac{\varepsilon_2}{2}\right]; \quad \sigma_2 = \frac{\bar{\sigma}}{\bar{\varepsilon}}\left[\varepsilon_2 + \frac{\varepsilon_2}{2}\right] \tag{11}$$

$$\alpha = \frac{\sigma_2}{\sigma_1} = \frac{[\varepsilon_2 + (1/2)\varepsilon_1]}{[\varepsilon_1 + (1/2)\varepsilon_2]} = \frac{[\beta + (1/2)]}{[1 + (1/2)\beta]} = \frac{2\beta + 1}{2 + \beta} \tag{12}$$

$$P = (1.67T^3 - 4T^2 + 3.33T)\frac{2t_i}{d_i - t_i}\frac{K\left((2/\sqrt{3})(1 + \beta + \beta^2)^{1/2}.\varepsilon_a\right)^n}{(1 - \alpha + \alpha^2)^{1/2}} \tag{13}$$

It should be noted that Eq. (13) represents initial pressure loading path for bulge tube hydroforming. Since the bulge analysis did not consider friction (free expansion analysis), and tube length, the pressure may not be adequate. Thus, this profile is used as initial input to FE simulation. Through FE iterations this pressure profile was scaled up to 1.35 to successfully form the Bulge shape with maximum thinning below 30%. To determine the pressure profile for the other THF families, Eq. (13) derived for the Bulge shape was used as an initial pressure curve and FE iterations were carried out to determine the scaling factors. Table 1 shows the scaling factors for all the families selected for this study. The scaling factors give satisfactory results within the following range of the parameters. Friction coefficient from $\mu = 0.001$ to $\mu = 0.25$ for all families, Length of the tube from 150 mm to 400 mm for Bulge, 150 mm to 300 mm for Single Y and Single T, 200 mm to 350 mm for Double

Please cite this article in press as: Ghosh, A., et al., Database for real-time loading path prediction for tube hydroforming using multidimensional cubic spline interpolation. J. Mater. Process. Tech. (2010), doi:10.1016/j.jmatprotec.2010.09.012

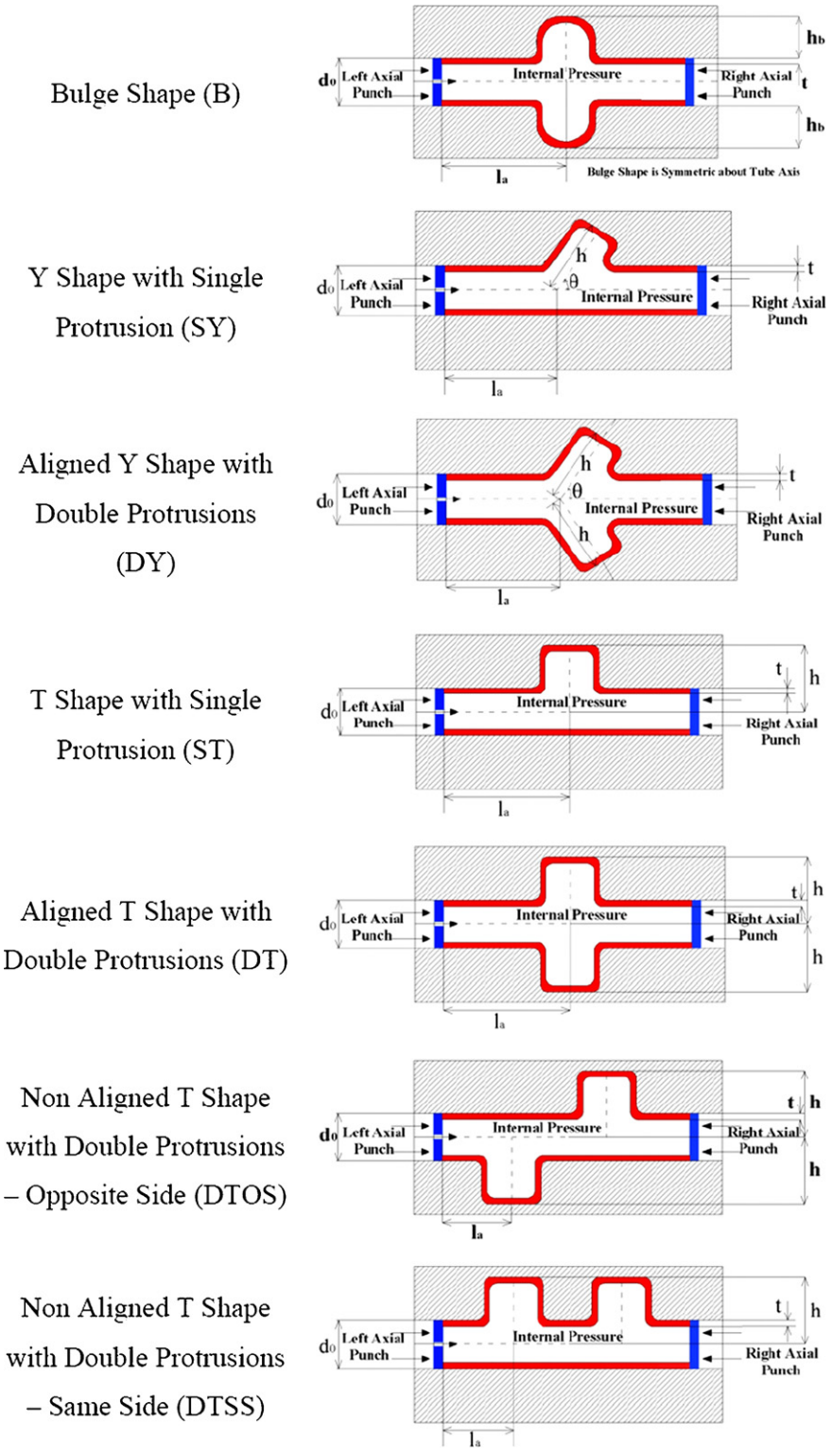


**Fig. 4.** THF families used in the database.

**Table 1**
Scaling factors for pressure curve generation.

| THF family | Scaling factor | THF family | Scaling factor |
|---|---|---|---|
| Bulge shape (B) | 1.35 | Aligned Double T shape (DT) | 2.45 |
| Single Y shape (SY) | 2.35 | Non Aligned Double T shape – opposite side (DTOS) | 2.45 |
| Aligned Double Y shape (DY) | 1.80 | Non Aligned Double T shape – same side (DTSS) | 2.00 |
| Single T shape (ST) | 2.45 | | |

Please cite this article in press as: Ghosh, A., et al., Database for real-time loading path prediction for tube hydroforming using multidimensional cubic spline interpolation. J. Mater. Process. Tech. (2010), doi:10.1016/j.jmatprotec.2010.09.012

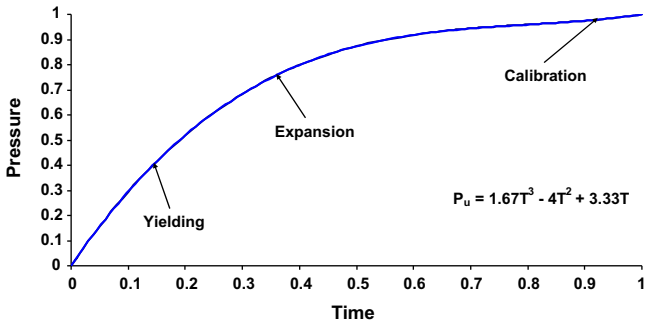


**Fig. 5.** Unit pressure profile.

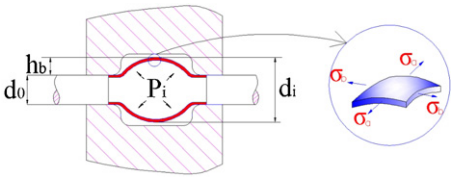


**Fig. 6.** Bulge shape THF.

Y and Aligned Double T, Double T unaligned same side (DTSS) and Double T unaligned opposite side (DTOS).

## 5. Axial feed curve generation using FEA

The THF process depends on the material, tribological and geometrical parameters. The following nine parameters from different categories are taken as the governing variables for this study.

*Material parameters*

Material strength coefficient, $K_{i_K} \in [a_K, b_K]$, where $i_K = 0, \ldots, n_K$

Strain hardening coefficient, $n_{i_n} \in [a_n, b_n]$, where $i_n = 0, \ldots, n_n$

*Tribological parameters*

Friction coefficient, $\mu_{i_\mu} \in [a_\mu, b_\mu]$, where $i_\mu = 0, \ldots, n_\mu$

*Geometrical parameters*

Initial outer diameter of the tube, $d_{i_d} \in [a_d, b_d]$, where $i_d = 0, \ldots, n_d$

Initial thickness of the tube, $t_{i_t} \in [a_t, b_t]$, where $i_t = 0, \ldots, n_t$

Initial length of the tube, $l_{i_l} \in [a_l, b_l]$, where $i_l = 0, \ldots, n_l$

Protrusion/bulge position along the length of the tube, $\times \quad l_a \in [a_{l_a}, b_{l_a}]$, where $i_{l_a} = 0, \ldots, n_{l_a}$

Protrusion/bulge height, $h_{i_h} \in [a_h, b_h]$, where $i_h = 0, \ldots, n_h$

Angle of the protrusion, $\theta_{i_\theta} \in [a_\theta, b_\theta]$, where $i_\theta = 0, \ldots, n_\theta$

The material feed data corresponding to all these nine variables are represented by $F_{i_K i_n i_\mu i_d i_t i_l i_{l_a} i_h i_\theta}$. However the material feed data itself is an array of 101 displacement values corresponding to the incremental time interval, i.e. $(F_{i_K i_n i_\mu i_d i_t i_l i_{l_a} i_h i_\theta})_{i_T}$, $i_T = 0, \ldots, 100$.

Table 2 shows the simulation matrix for the database development. However in order to analyze the data, additional sets of simulations were also carried out. As seen in Table 2, only one node is used for each of the last 6 dimensions namely $d$, $t$, $l$, $l_a$, $h$ and $\theta$ to reduce the number of simulations. In order to develop the database 27 sets of parameters for each family, adding up to 189 sets were chosen. The simulation parameters are presented in the following order with the specified unit unless otherwise mentioned. ($K$, $n$, $\mu$, $d$, $t$, $l$, $l_a$, $h$, $\theta$), where $K$ is in MPa; $d$, $t$, $l$, $l_a$ and $h$ are in mm; and $\theta$ is in°.

### 5.1. Inputs, boundary conditions, and FE results

The FEA analysis package used in this study is Abaqus 6.7, which is an explicit code. In the simulation, it is ensured that tube ends are always in contact with punches. The assumptions made for the simulations are rigid die and punch, deformable tube with shell type elements, simulation process time of 0.01 s and 30% maximum wall thinning. In this study $\bar{\sigma} = K\bar{\varepsilon}^n$ material model is selected and coefficient of friction ($\mu$) is prescribed at the tube-die/tube-punch

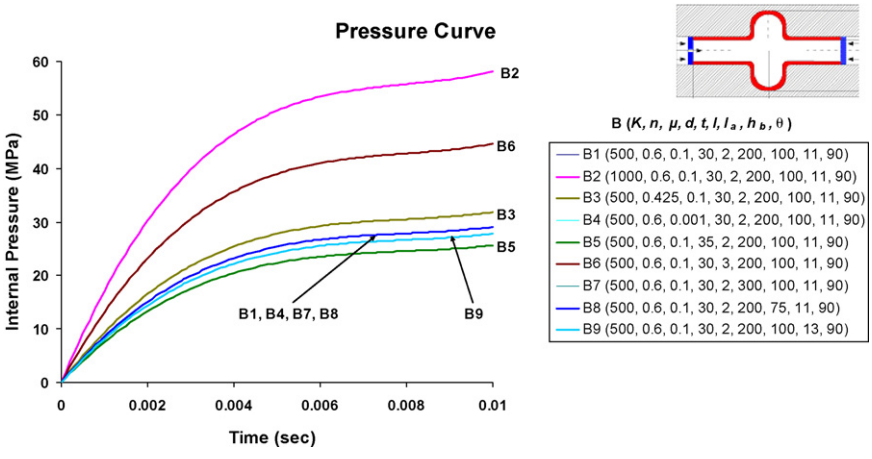


**Fig. 7.** Pressure curve variations for Bulge shape (B).

Please cite this article in press as: Ghosh, A., et al., Database for real-time loading path prediction for tube hydroforming using multidimensional cubic spline interpolation. J. Mater. Process. Tech. (2010), doi:10.1016/j.jmatprotec.2010.09.012

**Table 2**
Simulation matrix.

| Families | $K$ (MPa) | $n$ | $\mu$ | $d$ (mm) | $t$ (mm) | $l$ (mm) | $l_a$ (mm) | $h$ (mm) | $\theta$ (°) |
|---|---|---|---|---|---|---|---|---|---|
| Bulge shape (B) | 500<br>1000<br>1500 | 0.1<br>0.425<br>0.60 | 0.001<br>0.1<br>0.25 | {30} | {2} | {200} | {100} | {11} | {90} |
| Single Y shape (SY) | 500<br>1000<br>1500 | 0.1<br>0.425<br>0.60 | 0.001<br>0.1<br>0.25 | {30} | {2} | {150} | {70} | {36} | {60} |
| Aligned Double Y shape (DY) | 500<br>1000<br>1500 | 0.1<br>0.425<br>0.60 | 0.001<br>0.1<br>0.25 | {34.925} | {1.651} | {200} | {87.3} | {45} | {60} |
| Single T shape (ST) | 500<br>1000<br>1500 | 0.1<br>0.425<br>0.60 | 0.001<br>0.1<br>0.25 | {30} | {2} | {150} | {75} | {30} | {90} |
| Aligned Double T shape (DT) | 500<br>1000<br>1500 | 0.1<br>0.425<br>0.60 | 0.001<br>0.1<br>0.25 | {30} | {2} | {200} | {100} | {30} | {90} |
| Non Aligned Double T shape – opposite side (DTOS) | 500<br>1000<br>1500 | 0.1<br>0.425<br>0.60 | 0.001<br>0.1<br>0.25 | {30} | {2} | {200} | {50} | {30} | {90} |
| Non Aligned Double T shape – same side (DTSS) | 500<br>1000<br>1500 | 0.1<br>0.425<br>0.60 | 0.001<br>0.1<br>0.25 | {34.925} | {1.651} | {200} | {58.4} | {30} | {90} |

interface. Fluid pressure load was given uniformly to the inner surface of the tube. The punch velocity profiles to form an acceptable part were obtained by iterative simulations until an acceptable part is formed. The typical thickness variation maps for the different families are shown in Table 3.

The representative pressure curves, axial material feeds (displacement) are discussed for different families with respect to different variables. Fig. 7 shows the variation of the pressure curves for different variables for the Bulge family. These profiles are based on Eq. (13). From curves B1 and B2, it could be observed that, as

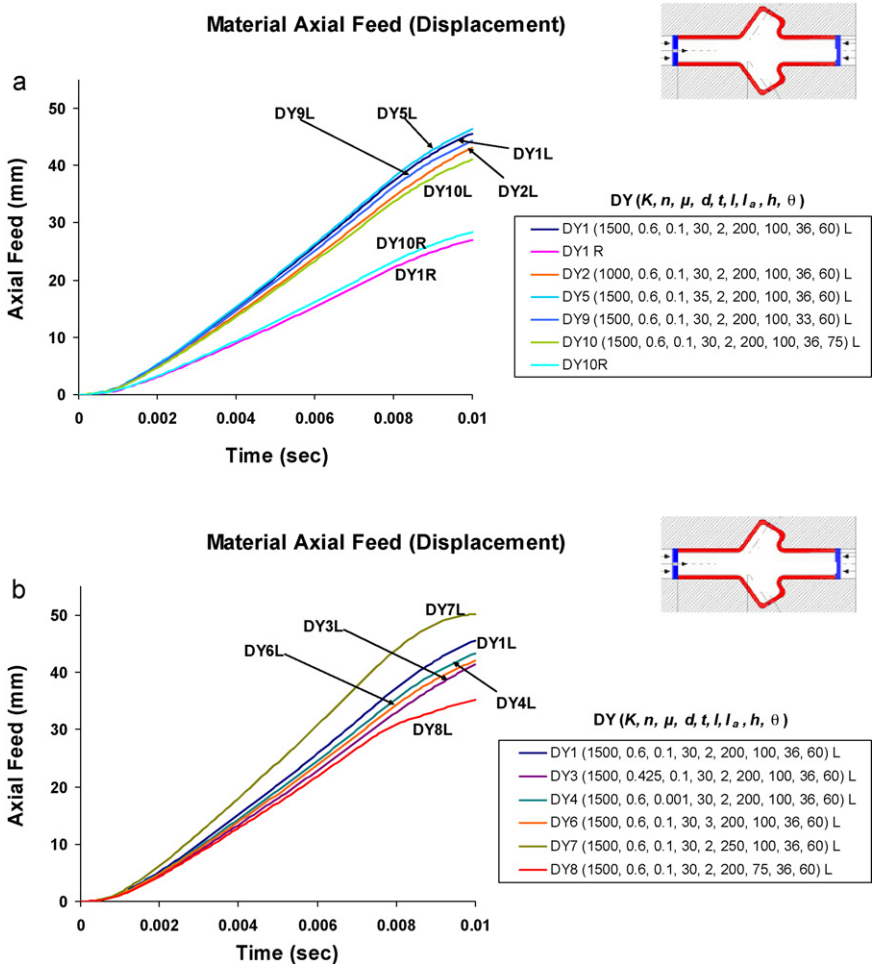


**Fig. 8.** (a) Material axial displacement feed variations for Aligned Double Y shape (DY) and (b) material axial displacement feed variations for Aligned Double Y shape (DY).

Please cite this article in press as: Ghosh, A., et al., Database for real-time loading path prediction for tube hydroforming using multidimensional cubic spline interpolation. J. Mater. Process. Tech. (2010), doi:10.1016/j.jmatprotec.2010.09.012

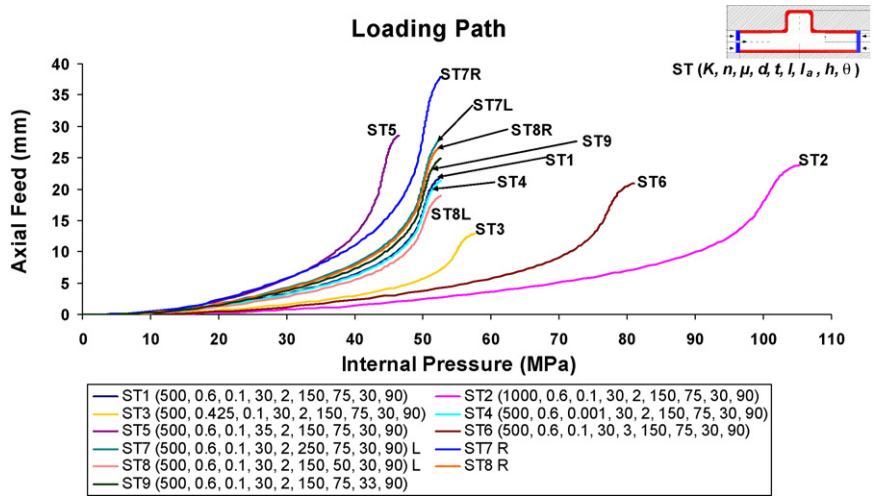


**Fig. 9.** Loading path variations for Single T shape (ST).

the value of strength coefficient $K$ increases, the internal pressure increases. This is due to the fact that the flow stress increased with increase in the strength coefficient, $K$. It is also found from curves B1 and B3 that the internal pressure increases with decrease in the strain hardening coefficient $n$. This is due to the fact that for a material that obeys the power law, lower $n$ value will results in higher stress at strain levels below 1.0.

In Fig. 7, the curves B1, B4, B7 and B8 fall into the same curve, since the variations of coefficient of friction ($\mu$), initial length of the tube ($l$) and the bulge position ($l_a$) are not included in the maximum instantaneous pressure Eq. (13). It should be noted, however, that the effects of $\mu$, $l$ and $l_a$ will be factored in the material feed curves. Since the initial diameter of the tube ($d$) and bulge height ($h_b$) are inversely proportional to the maximum instantaneous pressure, the pressure decreases with increasing $d$ and $h_b$ as shown by curves B1–B5 and B1–B9 respectively. As can be seen in Eq. (13) the initial tube thickness ($t$) is directly proportional to the maximum instantaneous pressure, thus the pressure increases with increasing $t$ as shown in the curves B1 and B6.

Fig. 8a and b shows the representative material displacement variation for DY family with respect to the change in the parameters. Curves DY1L and DY1R show that, the left axial feed is greater than the right axial feed. The same observation is found for asymmetric shape like SY. Since the Y protrusion is inclined towards the right side for both the SY and DY families, it is easier to feed the material from the left side for such geometry and so the left feed is greater than the right feed. The DTSS shape and the DTOS shape are always symmetric for all geometric variations, thus the material feed for both left and right sides is the same. However, the remaining families such as B, ST and DT could be either symmetric or asymmetric based on the geometry. When the position of the bulge/protrusion is at the center of the tube ($l_a = 0.5l$), the families are symmetric.

From DY1L and DY4L curves, it could be observed that material feed decrease with decrease in the coefficient of friction ($\mu$). This is attributed to the fact that with higher friction more material will be needed at the die cavity to compensate for rapid thinning. From curves DY1L and DY5L it could be observed that as the diameter of the tube ($d$) increases, the axial feed also increases. In case of a constant and uniform thinning, the axial feed does not change with variation of initial tube thickness ($t$). However some variations are observed in DY1L and DY6L, since the thinning is not constant and uniform. The axial feed increases with increasing initial tube length ($l$) and protrusion height ($h$) as seen in DY1L–DY7L and DY1L–DY9L respectively. The position of the protrusion ($l_a$) also changes the axial feed based on the symmetry of the THF part. From the curves DY1L and DY10L, it is found that with increasing protrusion angle ($\theta$), the axial feed reduces in the left side and increases in the right side. This is due to the fact that as the angle increases, the shape tends to be more symmetric. Finally the representative loading paths obtained from the pressure curves and the material axial feed curves, are shown in Fig. 9 for the ST family.

## 6. Data analysis and interpolation

### 6.1. Data analysis

In order to obtain continuous data for loading path in the specified range, the database developed need to be interpolated. In order to select an appropriate interpolation scheme the data was first analyzed. Most interpolation schemes require that the data be monotonic. Monotonic data is defined as that data which is either in an increasing order or in a decreasing order or that which remains the same. However, strictly monotonic data refers to the data being only in increasing or decreasing trend.

Figs. 10–13 show the representative material feed data variations with respect to the different variables for monotonicity. As seen in the figures the material feed data was found to be monotonic for all sets of simulations and for all time steps. Fig. 10 shows that the axial feed increases monotonically as material strength coefficient, $K$, increases. Similar trend is observed for strain hardening coefficient (Fig. 11). Fig. 12 shows that the right side material feed increases with increase in tube length for the Bulge shape. It

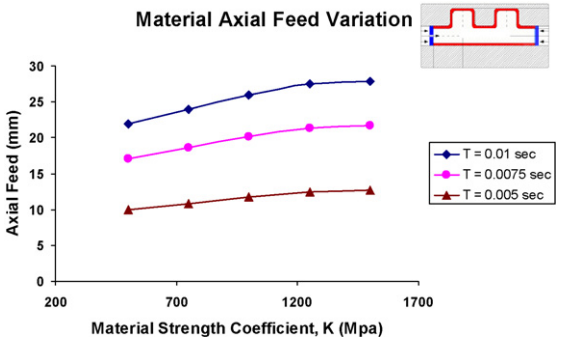


**Fig. 10.** Material axial displacement feed variations with respect to material strength coefficient ($K$); DTSS ($K$, 0.6, 0.1, 30, 2, 200, 50, 30, 90); values of $K$ are 500, 750, 1000, 1250 and 1500 MPa.

Please cite this article in press as: Ghosh, A., et al., Database for real-time loading path prediction for tube hydroforming using multidimensional cubic spline interpolation. J. Mater. Process. Tech. (2010), doi:10.1016/j.jmatprotec.2010.09.012

**Table 3**
Thickness variation.

| | |
|---|---|
| B (500, 0.6, 0.1, 30, 2, 200, 100, 11, 90) | 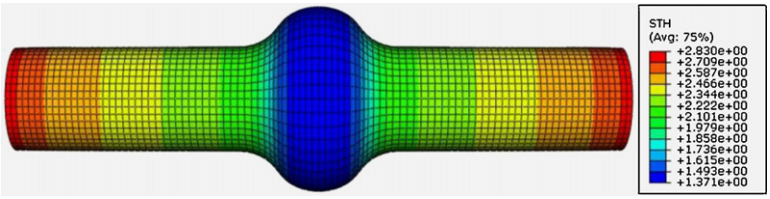  |
| SY (1500, 0.425, 0.1, 30, 2, 150, 70, 36, 60) | 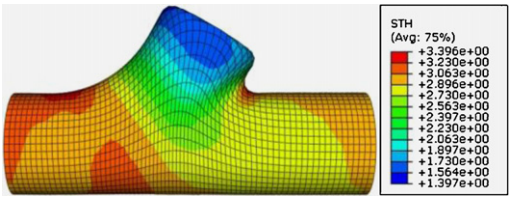  |
| DY (1500, 0.6, 0.001, 34.925, 1.651, 200, 87.3, 45, 60) | 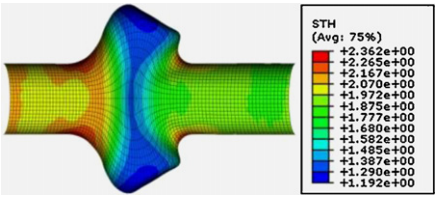  |
| ST (500, 0.6, 0.1, 30, 2, 150, 75, 30, 90) | 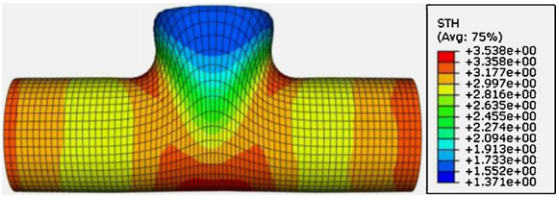  |
| DT (1500, 0.6, 0.001, 30, 2, 200, 100, 30, 90) | 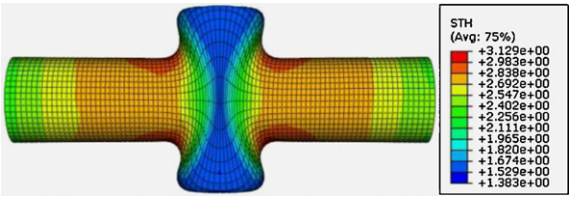  |
| DTOS (500, 0.6, 0.1, 30, 2, 200, 50, 30, 90) | 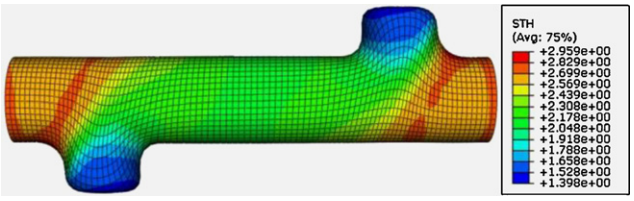  |
| DTSS (1500, 0.6, 0.001, 34.925, 1.651, 200, 58.4, 30, 90) | 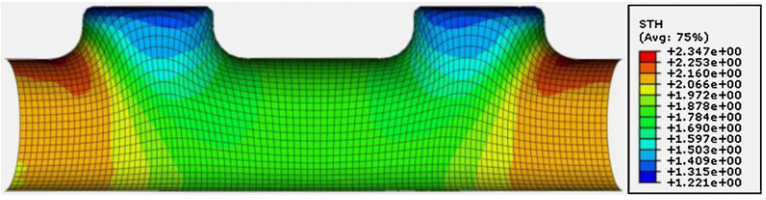  |

should be noted that due to non-symmetric of the part the left side material feed will decrease with increase in the tube length. Similar trend is observed with DY shape as the protrusion angle is varied as shown in Fig. 13.

The characteristic behavior of the data was also tested. The tests included (a) linear, (b) logarithmic, (c) polynomial, 2nd and 3rd order, (c) power, and (d) exponential. The accuracy of the approximation of a data set by a particular curve was quantified by a parameter known as the coefficient of determination ($R^2$), which varies from 0 to 1. The closer is the value of $R^2$ to 1, the better is the approximation. The coefficient of determination is defined by Eq. (14).

$$R^2 = 1 - \frac{\mathrm{SSE}}{\mathrm{SST}} \tag{14}$$

Please cite this article in press as: Ghosh, A., et al., Database for real-time loading path prediction for tube hydroforming using multidimensional cubic spline interpolation. J. Mater. Process. Tech. (2010), doi:10.1016/j.jmatprotec.2010.09.012

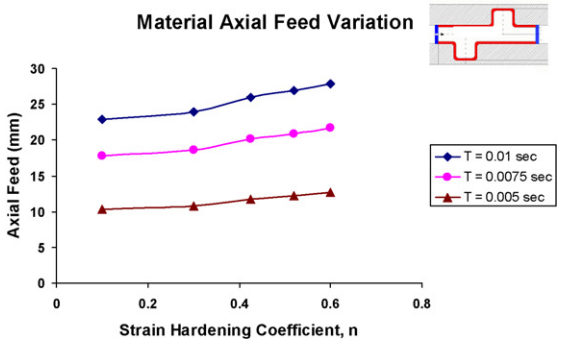


**Fig. 11.** Material axial displacement feed variations with respect to strain hardening coefficient ($n$); DTOS (1500, $n$, 0.1, 30, 2, 200, 50, 30, 90); values of $n$ are 0.1, 0.3, 0.425, 0.52 and 0.6.

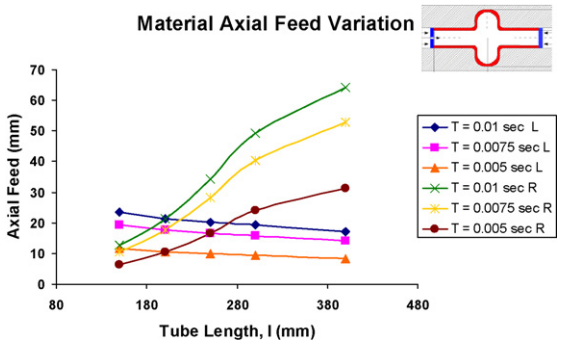


**Fig. 12.** Material axial displacement feed variations with respect to initial tube length ($l$); B (1500, 0.52, 0.1, 30, 2, $l$, 100, 11, 90); values of $l$ are 150, 200, 250, 300 and 400 mm.

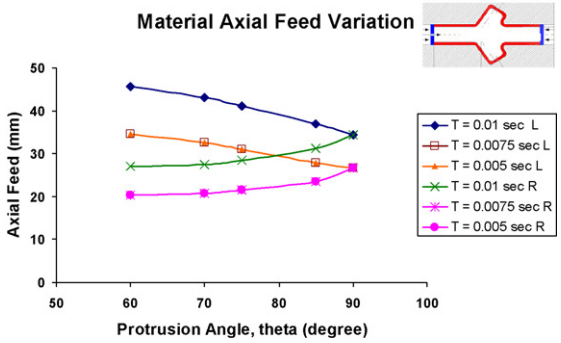


**Fig. 13.** Material axial displacement feed variations with respect to protrusion angle ($\theta$); DY (1500, 0.52, 0.1, 30, 2, 200, 100, 36, $\theta$); values of $\theta$ are 60°, 70°, 75°, 85° and 90°.

where $SSE = \sum (Y_i - \hat{Y}_i)^2$, $SST = \sum (Y_i^2) - ((\sum \Sigma Y_i)^2/N)$, $Y_i$ is the actual data, $\hat{Y}_i$ is the approximated data and $N$ is the number of data points.

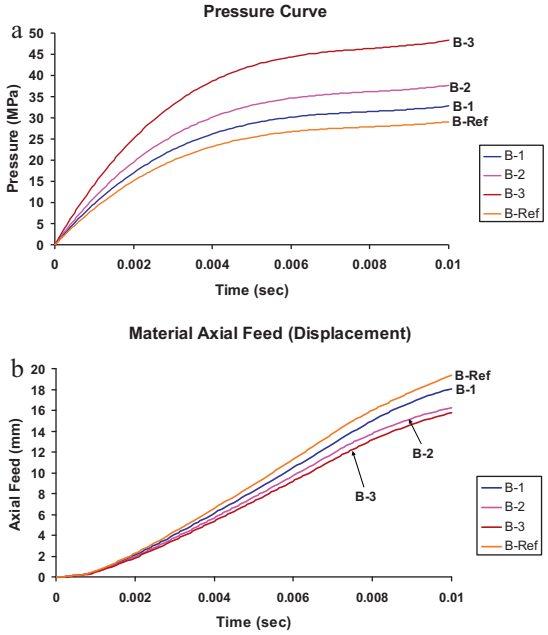


**Fig. 14.** (a) Pressure curves and (b) material axial feed vs. time.

Trend analysis was performed by choosing 5 nodes for each parameter variation. Table 4 shows the $R^2$ values for the trend analysis of the data. For the six types of curves tested, it is observed that the linear, logarithmic, power and the exponential curves fail to fit the data satisfactorily for all variables as their $R^2$ values are low. The polynomial curves give better approximations for all the variables.

### 6.2. Interpolation scheme – multidimensional cubic spline interpolation

Based on the data analysis presented above the cubic spline interpolation scheme is chosen to approximate the material feed function. Since the material feeds depend upon the nine variables namely material strength coefficient ($K$), strain hardening coefficient ($n$), friction coefficient ($\mu$), initial outer diameter of tube ($d$), initial thickness of the tube ($t$), initial length of the tube ($l$), the position of the protrusion/bulge along the length of the tube ($l_a$), protrusion/bulge height ($h$) and the protrusion angle ($\theta$); the problem becomes a multidimensional interpolation problem where the cubic spline approximation is to be used. It should be noted that except the Y-families the protrusion angle is constant and equal to 90°, which makes the interpolation problem for those families eight dimensional. However for generalization purpose nine-dimensional interpolation would be discussed. The cubic spline interpolation scheme used in this study is based on the work of Habermann and Kindermann (2007).

**Table 4**
$R^2$ values for trend analysis.

| Trend | $R^2$ value of material axial displacement feed data at $T = 0.01$ s | | | | | | | | | | | | |
|---|---|---|---|---|---|---|---|---|---|---|---|---|---|
| | $K$ | $n$ | $\mu$ | | $d$ | $t$ | $l$ | | $l_a$ | | $h$ | $\theta$ | |
| | | | Left | Right | | | Left | Right | Left | Right | | Left | Right |
| Linear | 0.9579 | 0.9617 | 0.8525 | 0.7804 | 0.9954 | 0.8441 | 0.9764 | 0.9841 | 0.9828 | 0.9449 | 0.9732 | 0.8606 | 0.9842 |
| Logarithmic | 0.9882 | 0.8314 | 0.9565 | 0.9850 | 0.9953 | 0.9540 | 0.9945 | 0.9765 | 0.9507 | 0.9760 | 0.9616 | 0.8175 | 0.9655 |
| 2nd order polynomial | 0.9943 | 0.9856 | 0.9714 | 0.8791 | 0.9968 | 0.9737 | 0.9919 | 0.9887 | 0.9945 | 0.9873 | 0.9808 | 0.9917 | 0.9994 |
| 3rd order polynomial | 0.9999 | 0.9968 | 0.9865 | 0.8929 | 0.9998 | 0.9978 | 0.9990 | 0.9999 | 0.9972 | 0.9874 | 0.9985 | 0.9988 | 0.9995 |
| Power | 0.9883 | 0.8457 | 0.9802 | 0.9838 | 0.9967 | 0.9607 | 0.9900 | 0.9807 | 0.9689 | 0.9824 | 0.9680 | 0.8363 | 0.9512 |
| Exponential | 0.9485 | 0.9669 | 0.8431 | 0.7417 | 0.9916 | 0.8556 | 0.9885 | 0.9228 | 0.9910 | 0.9613 | 0.9769 | 0.8778 | 0.9740 |

Please cite this article in press as: Ghosh, A., et al., Database for real-time loading path prediction for tube hydroforming using multidimensional cubic spline interpolation. J. Mater. Process. Tech. (2010), doi:10.1016/j.jmatprotec.2010.09.012

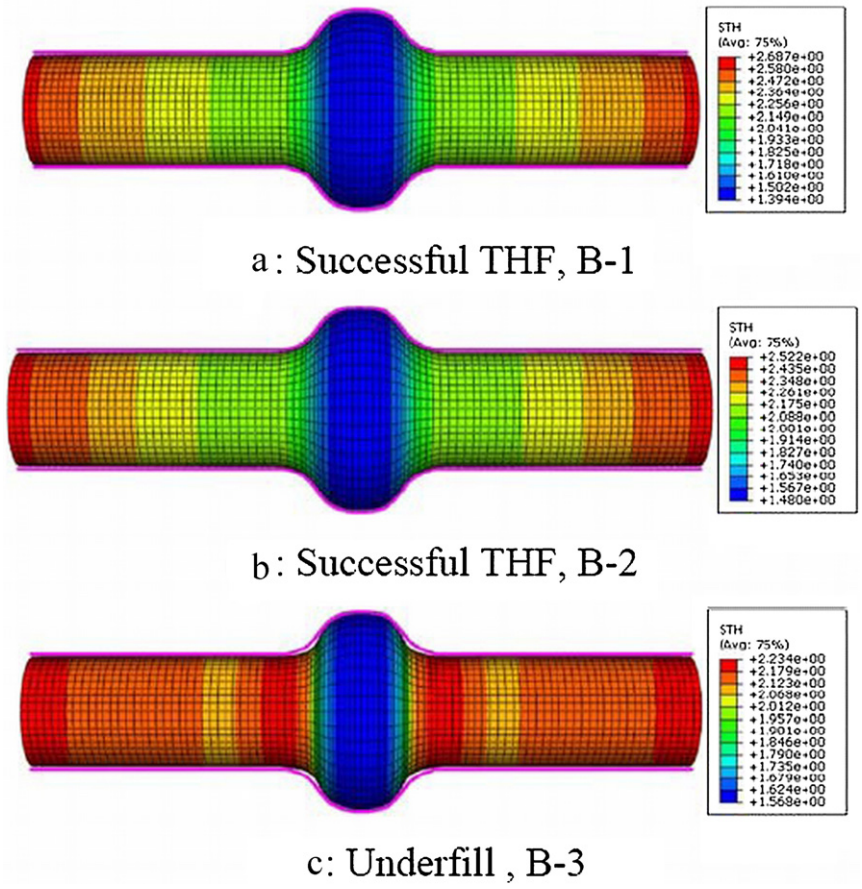


**Fig. 15.** Successful THF parts and a part with an under fill.

Here the nine variables are represented by the corresponding nine grids namely; $K$-grid for strength coefficient variable, $n$-grid for strain hardening coefficient variable, $\mu$-grid for friction coefficient, $d$-grid for initial outer diameter of tube, $t$-grid for initial thickness of tube, $l$-grid for initial length of tube, $l_a$-grid for the position of the protrusion/bulge along the length of tube, $h$-grid for protrusion/bulge height and $\theta$-grid for protrusion angle. The first grid $\Delta_K(a_K, b_K) = \{K_0, \ldots, K_{n_K}\}, n_K \in \mathbb{N}$ is defined on the interval $[a_K, b_K]$ as a set of points $K_{i_K} \in [a_K, b_K]$; where $i_K = 0, \ldots, n_K$, $a_K = K_0 \langle K_1 \langle \cdots \langle K_{n_K} = b_K$ and $K_{i_K}$ is the equidistant nodes. Here $\mathbb{N}$ refers to the set of Natural numbers {0, 1, 2, 3, ...}. For example if the database is generated for the material strength coefficient ($K$) values of {500, 750, 1000, 1250, 1500}MPa, then $\Delta_K(500, 1500) = \{K_0, K_1, K_2, K_3, K_4\} = \{500, 750, 1000, 1250, 1500\}$. The second grid is defined as $\Delta_n(a_n, b_n) = \{n_0, \ldots, n_{n_n}\}$, $n_n \in \mathbb{N}$ on the interval $[a_n,$

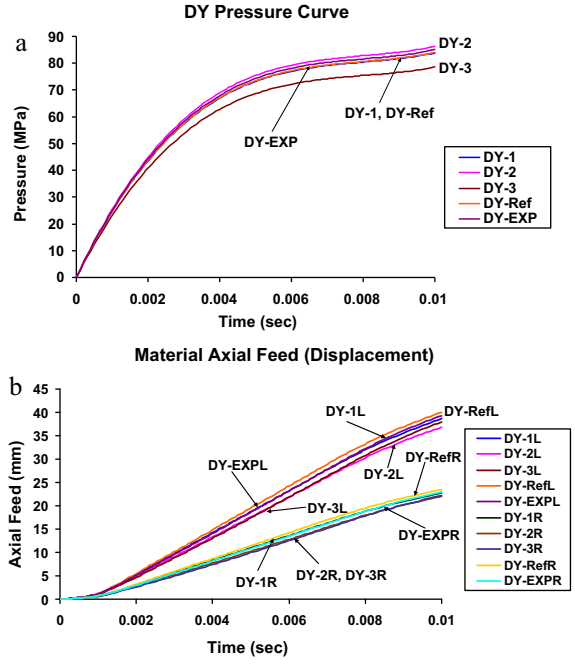


**Fig. 16.** (a) Pressure curves and (b) material axial feed vs. time.

**Table 5**
Interpolation scheme test data.

| | ($K$, $n$, $\mu$, $d$, $t$, $l$, $la$, $h$, $\theta$) |
|---|---|
| Bulge | |
| B-Ref | (500, 0.6, 0.1, 30, 2, 200, 100, 11, 90) |
| B-1 | (550, 0.55, 0.09, 30, 2, 200, 100, 11, 90) |
| B-2 | (600, 0.45, 0.08, 30, 2, 200, 100, 11, 90) |
| B-3 | (750, 0.40, 0.01, 30, 2, 200, 100, 11, 90) |
| Double Y | |
| DY-Ref | (1500, 0.6, 0.001, 34.925, 1.651, 200, 87.3, 45, 60) |
| DY-1 | (1450, 0.55, 0.005, 34.925, 1.651, 200, 87.3, 45, 60) |
| DY-2 | (1400, 0.45, 0.01, 34.925, 1.651, 200, 87.3, 45, 60) |
| DY-3 | (1275, 0.45, 0.05, 34.925, 1.651, 200, 87.3, 45, 60) |
| DY-EXP | (1426, 0.502, 0.05, 34.925, 1.651, 200, 87.3, 45, 60) |
| Double T same side | |
| DTSS-Ref | (1500, 0.6, 0.001, 34.925, 1.651, 200, 58.4, 30, 90) |
| DTSS-1 | (1450, 0.55, 0.005, 34.925, 1.651, 200, 58.4, 30, 90) |
| DTSS-2 | (1400, 0.45, 0.01, 34.925, 1.651, 200, 58.4, 30, 90) |
| DTSS-3 | (1275, 0.45, 0.05, 34.925, 1.651, 200, 58.4, 30, 90) |
| DTSS-EXP | (1426, 0.502, 0.05, 34.925, 1.651, 200, 58.4, 30, 90) |

Please cite this article in press as: Ghosh, A., et al., Database for real-time loading path prediction for tube hydroforming using multidimensional cubic spline interpolation. J. Mater. Process. Tech. (2010), doi:10.1016/j.jmatprotec.2010.09.012

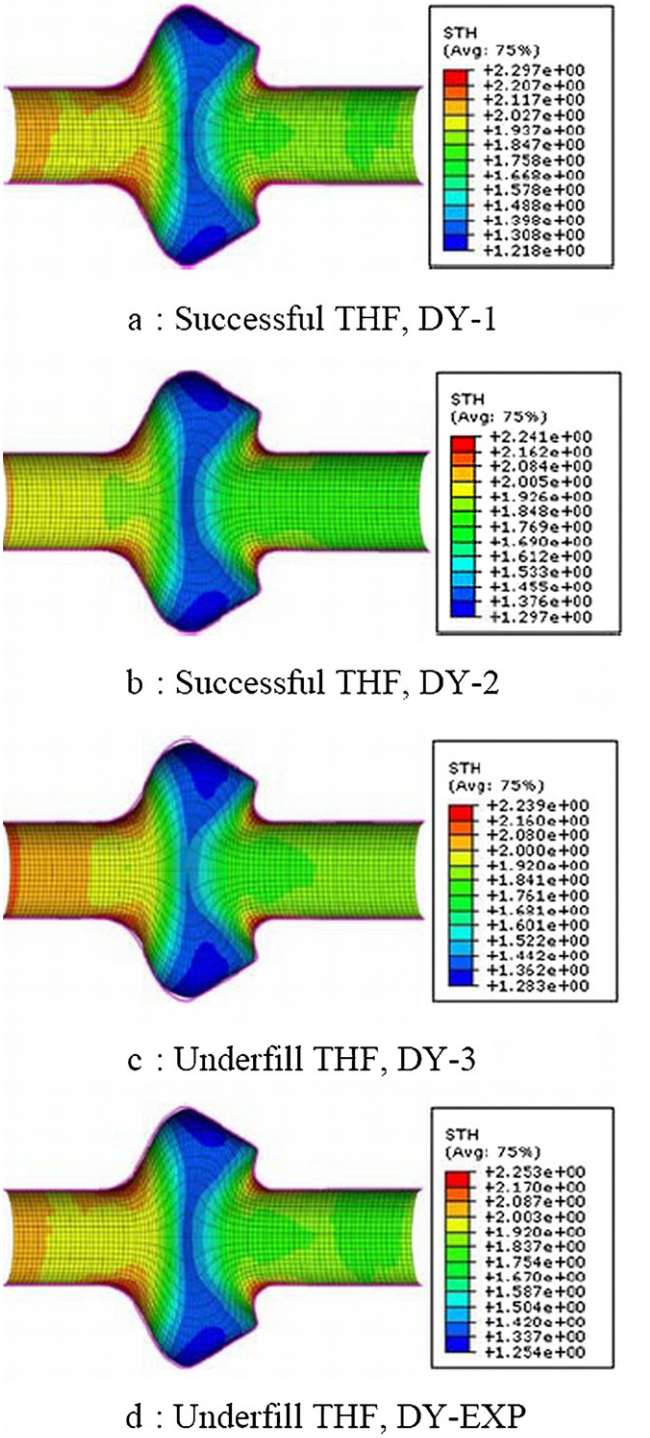


**Fig. 17.** Successful THF parts and parts with underfill.

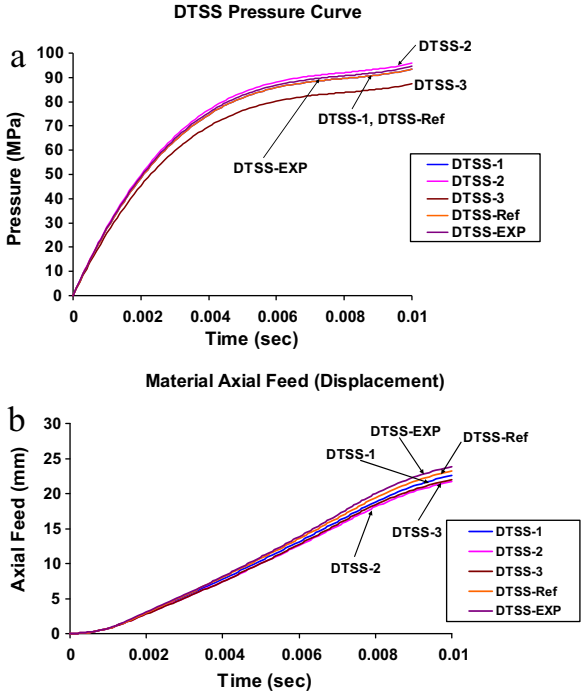


**Fig. 18.** (a) Pressure curves and (b) material axial feed vs. time.

$b_n]$ as a set of equidistant points $n_{i_n} \in [a_n, b_n]$; where $i_n = 0, \ldots, n_n$ and $a_n = n_0 \langle n_1 \langle \cdots \langle n_{n_n} = b_n$. In a similar fashion the remaining grids are defined. The interpolation data is the material feed and is defined as $F_{i_K i_n i_\mu i_d i_t i_l i_{l_a} i_h i_\theta} \in \mathbb{R}$; where $i_K = 0, \ldots, n_K$; $i_n = 0, \ldots, n_n$, $i_\mu = 0, \ldots, n_\mu$ and so on. Here $\mathbb{R}$ denotes the set of Real numbers. However the material feed data itself is an array of 101 displacement values corresponding to the incremental time interval, i.e. $(F_{i_K i_n i_\mu i_d i_t i_l i_{l_a} i_h i_\theta})_{i_T}$, $i_T = 0, 1, 2, \ldots, 100$. For example, the material feed required on the left side of the tube at time 0.01 s ($i_T = 100$) for Double Y-shape part is 45.63 mm for the forming conditions of $\{K, n, \mu, d, t, l, l_a, h, \theta\}$=$\{1500\,\text{MPa}, 0.6, 0.1, 30\,\text{mm}, 2\,\text{mm}, 200\,\text{mm}, 100\,\text{mm}, 36\,\text{mm}, 60^\circ\}$. This material feed data $F_{i_K i_n i_\mu i_d i_t i_l i_{l_a} i_h i_\theta}$ which is extracted from the simulation results is stored in the database.

In order to interpolate the material feed data $F_{i_K i_n i_\mu i_d i_t i_l i_{l_a} i_h i_\theta}$ stored in the database, a cubic spline of order three and smoothness two $s^{3,2}_{n_K,n_n,n_\mu,n_d,n_t,n_l,n_{l_a},n_h,n_\theta} \in S_{3,3,3,3,3,3,3,3,3}(\Delta_K, \Delta_n, \Delta_\mu, \Delta_d, \Delta_t, \Delta_l, \Delta_{l_a}, \Delta_h, \Delta_\theta)$, can be used, if it satisfies the interpolation conditions given by Eq. (15). Here $S_{3,3,3,3,3,3,3,3,3}(\Delta_K, \Delta_n, \Delta_\mu, \Delta_d, \Delta_t, \Delta_l, \Delta_{l_a}, \Delta_h, \Delta_\theta)$ is the function space of all splines of degree three and smoothness two on all grids. It should be noted that a spline of order three and smoothness two is a piecewise polynomial function with third order polynomial pieces. The polynomial pieces contain derivatives up to the second order.

$$s^{3,2}_{n_K,n_n,n_\mu,n_d,n_t,n_l,n_{l_a},n_h,n_\theta}(K_{i_K}, n_{i_n}, \mu_{i_\mu}, d_{i_d}, t_{i_t}, l_{i_l}, la_{i_{l_a}}, h_{i_h}, \theta_{i_\theta}) = F_{i_K i_n i_\mu i_d i_t i_l i_{la} i_h i_\theta} \quad (15)$$

Now using the B-Spline functions and the Natural Spline conditions, the interpolating spline $s$ could be defined as given in Eq. (16).

$$s(K, n, \mu, d, t, l, l_a, h, \theta) = \sum_{j_K}^{n_K+3n_n+3n_\mu+3n_d+3n_t+3n_l+3n_{l_a}+3n_h+3n_\theta+3} \sum_{j_n} \sum_{j_\mu} \sum_{j_d} \sum_{j_t} \sum_{j_l} \sum_{j_{l_a}} \sum_{j_h} \sum_{j_\theta} C_{j_K j_n j_\mu j_d j_t j_l j_{l_a} j_h j_\theta} u_{j_K}(K) u_{j_n}(n) u_{j_\mu}(\mu) u_{j_d}(d) u_{j_t} \times (t) u_{j_l}(l) u_{j_{l_a}}(l_a) u_{j_h}(h) u_{j_\theta}(\theta) \quad (16)$$

The coefficients $C_{j_K j_n j_\mu j_d j_t j_l j_{l_a} j_h j_\theta}$ are calculated in a structured way as detailed in Appendix A. Once the coefficients in Eq. (16) are known, the value of the spline for any sets of the nine variables ($K$, $n$, $\mu$, $d$, $t$, $l$, $l_a$, $h$, $\theta$) in the given interval could be obtained. This is the interpolated value of the material feed for that particular set of variables.

To illustrate the interpolation approach used in this study, a 2-diminsional cubic interpolation scheme is discussed in detail in

Please cite this article in press as: Ghosh, A., et al., Database for real-time loading path prediction for tube hydroforming using multidimensional cubic spline interpolation. J. Mater. Process. Tech. (2010), doi:10.1016/j.jmatprotec.2010.09.012

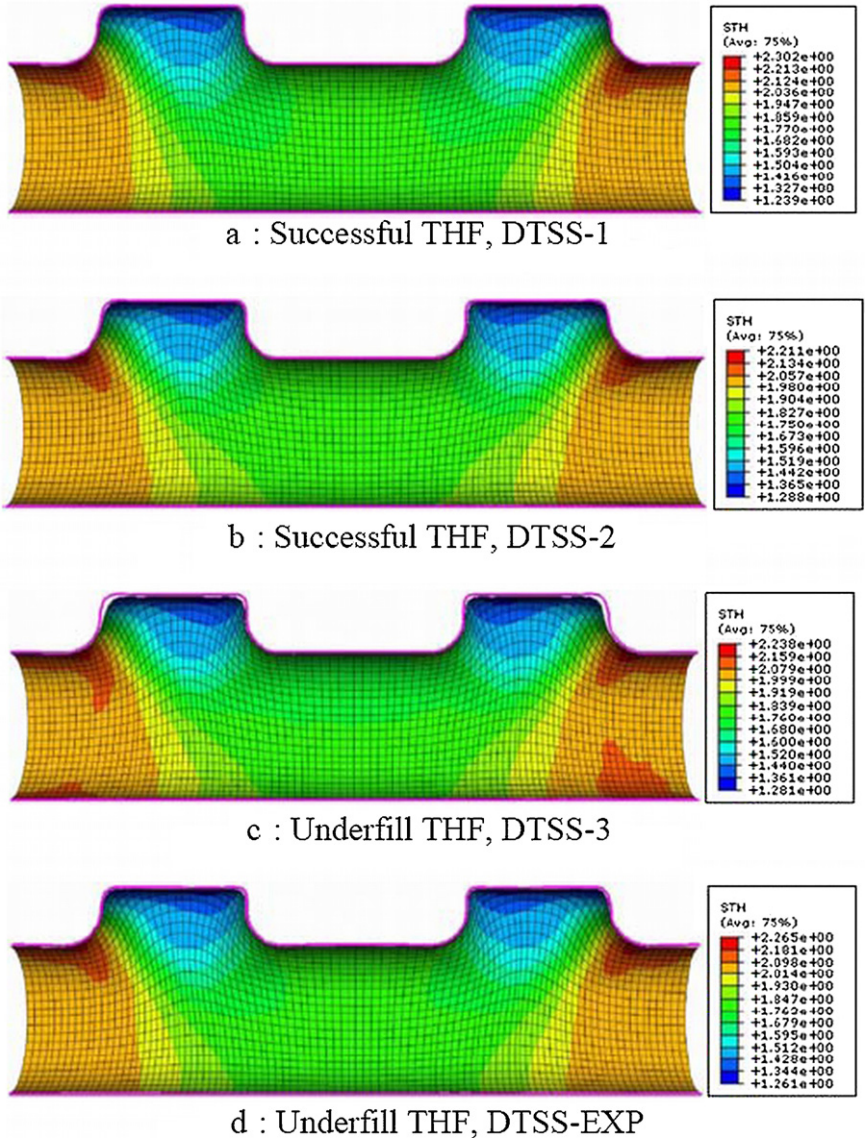


**Fig. 19.** Successful THF parts and parts with underfill.

the Appendix. For this illustration *K*-grid and *n*-grid variables were used.

## 7. Results and discussions

The loading paths (pressure vs. time, and material axial feed vs. time) established from the simulations for several THF families were used to build a database. The multidimensional cubic spline interpolation was used to determine the loading paths for any THF part that fell within the ranges of the variables used in the database. The database stored the data in a 9-dimensional matrix. The cubic spline interpolation scheme was carried out using Matlab and Visual BASIC. To check whether the loading paths produced by interpolation would lead to a successfully formed part, several tests were carried out. The tests also determined the maximum acceptable spacing of the data nodes. The user inputs were tested for the Bulge, Double Y, and Double T families, as shown in Table 5.

In Table 5, "Ref" represents an existing data node in the database, whereas "1", "2", and "3" refer to user-provided sets of parameters. "1" was the closest to "Ref", "2" was farther away from "Ref", and "3" bisected "Ref" and the adjacent existing data node. Hence the material feed data for "1", "2", and "3" were derived from the database using the multidimensional cubic spline interpolation. Furthermore, DY-EXP and DTSS-EXP are the sets used for experimental validation which will be discussed in the next section.

Fig. 14a and b shows the pressure curves and the material axial feeds for Bulge-shaped THF families B-Ref, B-1, B-2, and B-3. Fig. 15a–c shows the thickness variation obtained from simulations. These figures suggest that the interpolated axial-feed data yield satisfactory results for sets B-1 and B-2. However B-3 shows a slight underfill. The results imply that the spacing of the data nodes needs to be refined to provide an acceptable continuous loading path for the whole range. Therefore, it can be concluded that if the data nodes for the variables for the Bulge family were spaced at intervals of 100 MPa for *K*, 0.15 for *n*, and 0.02 for $\mu$, the database would

**Table 6**
Dimensional comparison of simulation and experiment.

| | Protrusion height from the center of the tube, *h* (mm) | |
|---|---|---|
| | Simulation | Experiment |
| DY | 43 | 42 |
| DTSS | 30 | 30 |

Please cite this article in press as: Ghosh, A., et al., Database for real-time loading path prediction for tube hydroforming using multidimensional cubic spline interpolation. J. Mater. Process. Tech. (2010), doi:10.1016/j.jmatprotec.2010.09.012

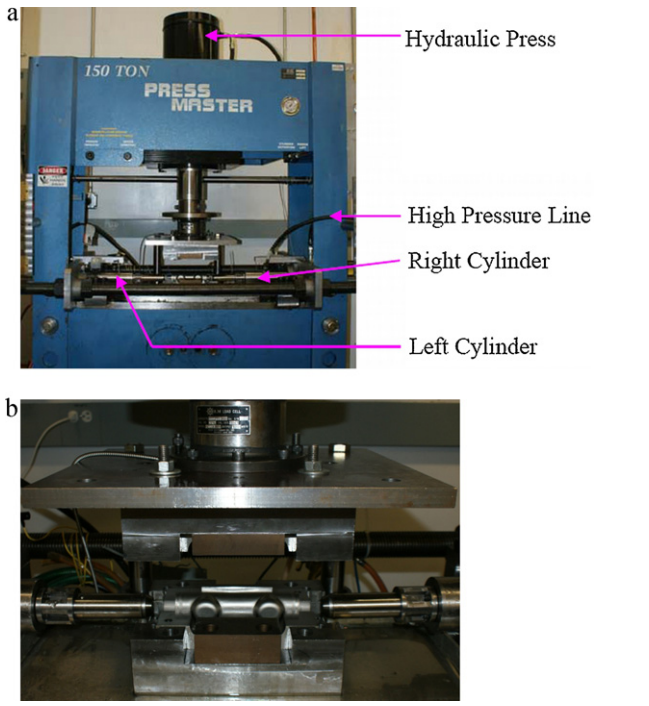


**Fig. 20.** (a) Hydroforming test rig and (b) tube hydroforming tooling.

give a loading path that forms the part satisfactorily for any set of parameters within the range.

Fig. 16a and b shows the pressure curves and the material axial feeds for Double-Y-shaped THF parts. Fig. 17a–d implies that DY-1 and DY-2 yield successful parts, whereas DY-3 and DY-EXP yield parts with underfill. This implies that the data nodes for Y-shape families should be spaced at intervals of 100 MPa for $K$, 0.15 for $n$, and 0.01 for $\mu$.

Fig. 18a and b shows the pressure curves and the material axial feeds for Non-aligned Double T shape – same-side (DTSS) THF parts. Fig. 19a–d shows that the DTSS-1 and DTSS-2 set give satisfactory results, whereas DTSS-3 and DTSS-EXP fail to form acceptable parts. Hence DTSS families will also require data node spacing of 100 MPa for $K$, 0.15 for $n$, and 0.01 for $\mu$.

## 8. Experimental validation

In order to validate the proposed methodology, THF experiments for aligned Double Y shape (DY) and Non-aligned double T-shape (DTSS) families were carried out. The loading paths used in the experiment were obtained by multidimensional interpolation scheme.

### 8.1. Test set-up and experimental procedures

The experimental set-up for THF is shown in Fig. 20a and b. The tooling set-up consists of split dies and die holders for DY and DTSS families, two axial cylinders (50 t capacity each) to provide the axial feed, and a 150 t hydraulic press which is used to clamp the split dies during the operation. The maximum fluid pressure that can be attained in this hydroforming test rig is 20,000 psi (140 MPa). The split dies were made of A2 steel and hardened to 62 HRC. Fig. 21a and b shows the cross-section views of the split dies showing the dimensions, which actually are the part dimensions sought to be achieved by the experiments. The tubular material used for the tests was stainless steel SS304 with material strength coefficient $K = 1426$ MPa and the strain hardening exponents $n = 0.502$. The dimensions of the tube samples are given in Table 5.

Prior to the experiments, the tube and the dies surfaces were cleaned by acetone. Lubrication was provided by a Teflon sheet which was wrapped around the tube. For both DY and DTSS THF experiments, the friction coefficient at the interface was estimated as 0.05 for the applied Teflon sheet. The loading paths used for these experiments were obtained from the database using the developed interpolation scheme. All the experiments were carried out in 20 s. It should be noted that all the loading paths residing in the database were obtained at a simulation time of 0.01 s. The difference in the process time should not account for any errors because the loading path for cold forming is independent of the process time.

### 8.2. Experimental results and discussions

The hydroformed parts DY and DTSS are shown in Fig. 22a and b, respectively. The dimensions of the protruded sections were measured and compared with the dimensions obtained from the FE simulations as shown in Table 6. The protrusion height of DTSS part matched very well between experiment and FE simulations. The protrusion height measured from DY hydroformed part was found to be 1 mm less than the protrusion height obtained from the simulation. The deviation may be attributed to non-linear friction exhibited at the interface. As mentioned earlier, a friction coefficient of 0.05 was assumed in the simulation. A slight increase in the interface friction has the propensity to hinder material flow to the die cavity. For the DY part more material was supposed to be fed from the left side. Hence, the effect of friction was more pronounced with this geometry compared to the DTSS geometry.

Wall thickness distribution for the DTSS and DY parts was also compared between experiment and FE simulations as shown in Fig. 23a and b. The thickness measurements were taken using Vernier caliper after cutting the specimens along the longitudinal direction. The thickness distribution plots only show measured values from the protrusion side of the parts. It can be seen that the thickness distributions obtained from the experiments closely match FE simulation results. The percentage difference between

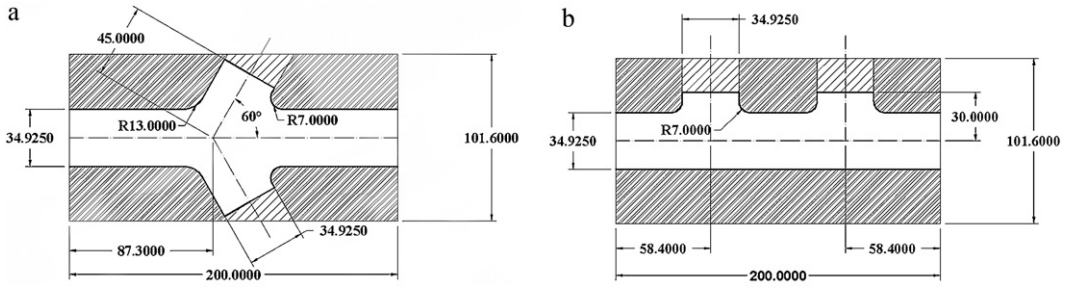


**Fig. 21.** (a) Cross-section of DY die, dimensions are in mm and (b) cross-section of DTSS die, dimensions are in mm.

Please cite this article in press as: Ghosh, A., et al., Database for real-time loading path prediction for tube hydroforming using multidimensional cubic spline interpolation. J. Mater. Process. Tech. (2010), doi:10.1016/j.jmatprotec.2010.09.012

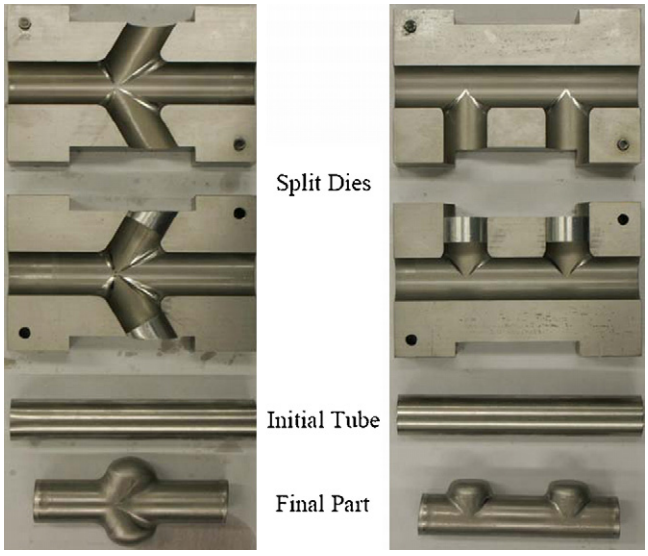


**Fig. 22.** Split dies, initial tube and final part for (a) DY-EXP and (b) DTSS-EXP.

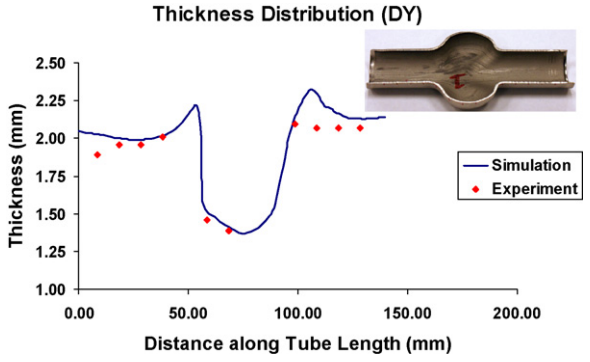


**Fig. 23.** (a) Thickness distribution comparison for DY part, final part length 138.5 mm and (b) thickness distribution comparison for DTSS part, final part length 152.6 mm.

experiment and simulation falls in the range from 0 to +10% for the DY case and in −6.6% to +6.2% for the DTSS case.

## 9. Conclusions

A database scheme for real-time loading-path prediction for THF parts was developed. The database contained material axial feed for a wide variety of THF components. THF parts were classified into families based on the geometrical configurations. The THF families identified were Bulge, Single Y, Aligned Double Y, Single T, Aligned Double T, Non-aligned Double T – opposite side, and Non-aligned Double T – same side. In order to obtain the loading path for these THF families, consideration was given to geometric parameters, material parameters, and tribological parameters. With the aid of FEA, simulations were carried out to establish the loading paths. The variations of axial feed with respect to all variables were analyzed for monotonicity, which is one of the critical conditions for determining appropriate interpolation. The cubic spline interpolation was employed to provide a real-time loading path. The validation of the proposed interpolation scheme was carried out in two stages. In stage one, the interpolated loading paths were validated using FEA. That is, FEA was carried out using the interpolated loading paths and then the formed geometry was assessed to determine if the part is successfully formed. The second validation was carried out by actual THF experiments for DY and DTSS families.

The following conclusions are drawn from this study:

- Material feed data obtained from FE simulations have shown to vary monotonically for all parameters (geometric, material, and tribological), irrespective of THF family. This indicates that multidimensional interpolation of the data to obtain the loading paths could be done with high precision.
- The tested data to obtain the loading paths for various THF families reveal that the interpolated loading paths are accurate if the node-spacing interval is appropriate. Bulge-shaped parts require node spacing intervals of 100 MPa for $K$, 0.15 for $n$, and 0.02 for $\mu$. Y-shaped parts require 100 MPa for $K$, 0.15 for $n$, and 0.01 for $\mu$. T-shaped parts also require 100 MPa for $K$, 0.05 for $n$, and 0.01 for $\mu$.
- Experiments carried out for DY and DTSS families have shown that the loading paths determined through the cubic spline interpolation scheme results in the part geometries that are very close to the ones predicted by FEA.
- Multidimensional cubic spline interpolation allows the database to output the required loading path within 0.85 s using Microsoft Windows XP Professional x64 Edition, Version 2003; Intel® Xeon® 4 CPU at 2.33 GHz; and 16.0 GB of RAM.

The method presented in this study to determine loading paths for THF parts could reduce the cost and time incurred in THF operations. Furthermore, this method eliminates the need for running multiple FE simulations for similar parts.

## Acknowledgments

The authors would like to acknowledge the National Science Foundation, through which this work was funded under Project No. DMI-0448885. Any opinions, findings, and conclusions or recommendations expressed in this material are those of the authors and do not necessarily reflect the views of the National Science Foundation

## Appendix A. 2-Dimensional cubic spline interpolation

To illustrate the interpolation scheme used in this study, material strength coefficient ($K$) and strain hardening coefficient ($n$) are chosen as variables, hence two grids namely $K$-grid and $n$-grid will be used. The first grid $\Delta_K(a_K, b_K) = \{K_0, \ldots, K_{n_K}\}$, $n_K \in \mathbb{N}$ is defined on the interval $[a_K, b_K]$ as a set of points $K_{i_K} \in [a_K, b_K]$; where $i_K = 0, \ldots, n_K$, $a_K = K_0 \langle K_1 \langle \cdots \langle K_{n_K} = b_K$ and $K_{i_K}$ is the equidistant nodes. Similarly the second grid is defined as $\Delta_n(a_n, b_n) = \{n_0, \ldots, n_{n_n}\}$, $n_n \in \mathbb{N}$ on the interval $[a_n, b_n]$ as a set of equidistant points $n_{i_n} \in [a_n, b_n]$; where $i_n = 0, \ldots, n_n$ and $a_n = n_0 \langle n_1 \langle \cdots \langle n_{n_n} = b_n$. The interpolation data is the material feed and is defined as $F_{i_K i_n} \in \mathbb{R}$; where $i_K = 0, \ldots, n_K$ and $i_n = 0, \ldots, n_n$. However the material data itself is an array of 101 displacement values corresponding to incremental time interval, i.e. $(F_{i_K i_n})_{i_T}$, $i_T = 0, \ldots, 100$.

Now a so-called cubic spline of order three and smoothness two $s^{3,2}_{n_K, n_n} \in S_{3,3}(\Delta_K, \Delta_n)$, where $S_{3,3}(\Delta_K, \Delta_n)$ is the function space of all degree three and smoothness two splines on both $K$ and $n$ grids, interpolates the data $F_{i_K i_n}$, if it satisfies the $(n_K + 1) \times (n_n + 1)$ interpolation conditions. Although the cubic spline which is a piecewise third-order polynomial could be calculated by an intuitive approach, it has certain disadvantages based on computation time and effort. To overcome this problem, the notion of basis functions of function space $S_{3,3}(\Delta_K, \Delta_n)$ is introduced where B-Spline functions are the most commonly used basis functions (De Boor,

Please cite this article in press as: Ghosh, A., et al., Database for real-time loading path prediction for tube hydroforming using multidimensional cubic spline interpolation. J. Mater. Process. Tech. (2010), doi:10.1016/j.jmatprotec.2010.09.012

2001).

$$s^{3,2}_{n_K n_n}(K_{i_K}, n_{i_n}) = F_{i_K i_n}, \quad \text{where } i_K = 0, \ldots, n_K \text{ and } i_n = 0, \ldots, n_n \tag{A.1}$$

$$B^{3,\Delta_K}_{j_K}(K) = \frac{K - K_{(j_K-1)-3}}{K_{(j_K-1)} - K_{(j_K-1)-3}} B^{3-1,\Delta_K}_{(j_K-1)}(K) + \frac{K_{j_K} - K}{K_{j_K} - K_{j_K-3}} B^{3-1,\Delta_K}_{j_K}(K) \tag{A.2}$$

$$\text{where, } j_K = 1, \ldots, n_K + 3 \text{ and } B^{0,\Delta_K}_{j_K} = \begin{cases} 1 & \text{if } K_{j_K-1} \le K \le K_{j_K} \\ 0 & \text{otherwise} \end{cases}$$

$$B^{3,\Delta_n}_{j_n}(n) = \frac{n - n_{(j_n-1)-3}}{n_{(j_n-1)} - n_{(j_n-1)-3}} B^{3-1,\Delta_n}_{(j_n-1)}(n) + \frac{n_{j_n} - n}{n_{j_n} - n_{j_n-3}} B^{3-1,\Delta_n}_{j_n}(n) \tag{A.3}$$

$$\text{where, } j_n = 1, \ldots, n_n + 3 \text{ and } B^{0,\Delta_n}_{j_n} = \begin{cases} 1 & \text{if } n_{j_n-1} \le n \le n_{j_n} \\ 0 & \text{otherwise} \end{cases}$$

Now the $n_K + 3$ B-Spline basis functions $B^{3,\Delta_K}_{j_K}$ and $n_n + 3$ B-Spline basis functions $B^{3,\Delta_n}_{j_n}$ form a basis of the function space $S_{3,3}(\Delta_K, \Delta_n)$. The cubic spline $s^{3,2}_{n_K,n_n}$ or simply $s_{n_K n_n}$ could therefore be presented as the linear combination of the tensor products of B-Spline basis functions on grid $\Delta_K$ and $\Delta_n$ with coefficients $C_{j_K j_n}$.

$$s^{3,2}_{n_K,n_n}(K, n) = \sum_{j_K=1}^{n_K+3} \sum_{j_n=1}^{n_n+3} C_{j_K j_n} B^{3,\Delta_K}_{j_K}(K) B^{3,\Delta_n}_{j_n}(n) \tag{A.4}$$

If Eqs. (A.1) and (A.4) are equated, they would yield the values of coefficients $C_{j_K j_n}$ and with the known values of $C_{j_K j_n}$, the value of any $s^{3,2}_{n_K n_n}(K, n)$ within the interval $[a_K, b_K]$ and $[a_n, b_n]$ could be calculated which is the interpolated value of material feed $F$ at that point $(K, n)$. Here the equidistant data nodes are chosen, so that the following equations could be written.

$$K_{i_K} = a_K + i_K h_K; \quad \text{interval}\,[a_K, b_K]; \quad h_K = \frac{b_K - a_K}{n_K}; \quad i_K = 0, \ldots, n_K \tag{A.5}$$

$$n_{i_n} = a_n + i_n h_n; \quad \text{interval}\,[a_n, b_n]; \quad h_n = \frac{b_n - a_n}{n_n}; \quad i_n = 0, \ldots, n_n \tag{A.6}$$

Now for equidistant nodes, the B-Splines shown in Eq. (A.4) could be explicitly presented in terms of some functions $u$.

$$B^{3,\Delta_K}_{j_K}(K) = u_{j_K}(K) = \Phi\left[\frac{K - a_K}{h_K} - j_K + 2\right], \quad \text{where } j_K = 1, \ldots, n_K + 3 \tag{A.7}$$

$$B^{3,\Delta_n}_{j_n}(n) = u_{j_n}(n) = \Phi\left[\frac{n - a_n}{h_n} - j_n + 2\right], \quad \text{where } j_n = 1, \ldots, n_n + 3 \tag{A.8}$$

$$\text{where, } \Phi(t) = \begin{cases} (2 - |t|)^3, & 1 \le |t| \le 2 \\ 4 - 6|t|^2 + 3|t|^3, & |t| \le 1 \\ 0, & \text{elsewhere} \end{cases}$$

Though one can use different $\Phi$ functions, there could be some variation in the numerical answers which would not be significant. Eq. (A.4) could thus be re-written as follows.

$$s^{3,2}_{n_K,n_n}(K, n) = \sum_{j_K=1}^{n_K+3} \sum_{j_n=1}^{n_n+3} C_{j_K j_n} u_{j_K}(K) u_{j_n}(n) \tag{A.9}$$

Since $u_{j_K}$ and $u_{j_n}$ vanish outside the respective bounded interval $[K_{j_K-4}, K_j] \cap [a_K, b_K]$ and $[n_{j_n-4}, n_{j_n}] \cap [a_n, b_n]$ due to the bounded support supp $(u_{j_K}) = [K_{j_K-4}, K_{j_K}] \cap [a_K, b_K]$ and supp $(u_{j_n}) = [n_{j_n-4}, n_{j_n}] \cap [a_n, b_n]$, Eq. (A.9) is further changed to the following form.

$$s^{3,2}_{n_K,n_n}(K, n) = \sum_{j_K=l_K}^{m_K} \sum_{j_n=l_n}^{m_n} C_{j_K j_n} u_{j_K}(K) u_{j_n}(n) \tag{A.10}$$

where $l_K = \lfloor (K - a_K)/h_K \rfloor + 1$, $m_K = \min(l_K + 3, n_K + 3)$, $l_n = \lfloor (n - a_n)/h_n \rfloor + 1$, $m_n = \min(l_n + 3, n_n + 3)$; $\lfloor \bullet \rfloor$ denotes the floor function.

The required equations for 2-dimensional cubic spline interpolations are defined and now the procedure to obtain the interpolated value of material feed $F$ at the point $(K, n)$ in the defined boundary is presented below in steps.

*Step 1*: The first step is to calculate the coefficients $C^*_{j_K q}$ of the following splines.

$$s_{q,K}(K) = \sum_{j_K=1}^{n_K+3} C^*_{j_K q} u_{j_K}(K) \quad \in S_3(\Delta_K) \tag{A.11}$$

where $q = 0, \ldots, n_n$ and the interpolation condition is,

$$s_{q,K}(K) = F_{i_K q}, \quad \text{where } i_K = 0, \ldots, n_K \tag{A.12}$$

Since $S_3(\Delta_K)$ is in $n_K + 3$ dimensional space, $n_K + 3$ interpolation conditions are required to calculate the unique interpolating spline function. However from Eq. (A.13) only $n_K + 1$ conditions are found. In order to get the remaining conditions the second-order derivatives of the spline function at the two boundaries are equated with some constants. If the spline is assumed as 'Natural Spline' then these constants would be zero (Behforooz and Papamichael, 1979). Finally Eq. (A.11) could be re-written as Eq. (A.15) in terms of known values.

$$s''_{q,K}(K_0) = \sum_{j_K=1}^{3} C^*_{j_K q} u''_{j_K}(K_0) = 0 \tag{A.13}$$

$$s''_{q,K}(K_{n_K}) = \sum_{j_K=n_K+1}^{n_K+3} C^*_{j_K q} u''_{j_K}(K_{n_K}) = 0 \tag{A.14}$$

$$s_{q,K}(K_{i_K}) = \sum_{j_K=l_K}^{m_K} C^*_{j_K q} u_{j_K}(K_{i_K}) \tag{A.15}$$

where $q = 0, \ldots, n_n$, $l_K = \lfloor (K_{i_K} - a_K)/h_K \rfloor + 1$, $m_K = \min(l_K + 3, n_K + 3)$, $i_K = 0, \ldots, n_K$.

After re-arranging Eqs. (A.13), (A.14) and (A.15) and also using Eq. (A.12), the following matrix equation is written, which could be

solved for the $C^*_{j_K q}$.

$$\begin{pmatrix} u''_1(K_0) & u''_2(K_0) & u''_3(K_0) & 0 & \cdots & \cdots & 0 \\ u_1(K_0) & u_2(K_0) & u_3(K_0) & u_4(K_0) & \cdots & \cdots & 0 \\ 0 & u_2(K_1) & u_3(K_1) & u_4(K_1) & u_5(K_1) & \cdots & 0 \\ \vdots & \ddots & \ddots & \ddots & \ddots & \ddots & \vdots \\ 0 & \cdots & 0 & u(K_{n_K-1}) & u(K_{n_K-1}) & u(K_{n_K-1}) & u(K_{n_K-1}) \\ 0 & \cdots & \cdots & 0 & u(K_{n_K}) & u(K_{n_K}) & u(K_{n_K}) \\ 0 & \cdots & \cdots & \cdots & u''_{n_K+1}(K_{n_K}) & u''_{n_K+2}(K_{n_K}) & u''_{n_K+3}(K_{n_K}) \end{pmatrix} \begin{pmatrix} C^*_{1q} \\ C^*_{2q} \\ C^*_{3q} \\ \vdots \\ C^*_{n_K+1q} \\ C^*_{n_K+2q} \\ C^*_{n_K+3q} \end{pmatrix} = \begin{pmatrix} 0 \\ F_{0q} \\ F_{1q} \\ \vdots \\ F_{n_K-1q} \\ F_{n_K q} \\ 0 \end{pmatrix} \tag{A.16}$$

*Step 2*: The second step is to solve the cubic spline interpolation problem $s_{j_K,n} \in S_3(\Delta_n)$.

$$s_{j_K,n}(n) = \sum_{j_n=1}^{n_n+3} C_{j_K j_n} u_{j_n}(n), j_K = 1, \ldots, n_K + 3 \tag{A.17}$$

and the interpolation condition is,

$$s_{j_K,n}(n_q) = C^*_{j_K q}, q = 0, \ldots, n_n \tag{A.18}$$

With similar reasoning and approaches, the value of $C_{j_K j_n}$ could be obtained using Eqs. (A.17) and (A.18).

*Step 3*: Since the coefficients $C_{j_K j_n}$ in Eq. (A.9) are known, for any $(K, n)$ value in the given interval, the corresponding spline could be calculated, which is the cubic spline interpolated value of the material feed $(F)$ at that particular $(K, n)$. Eq. (A.9) could be presented in matrix notation as expressed in Eq. (A.19), where $u_{j_K}(K)$, $u_{j_n}(n)$ and $C_{j_K j_n}$ denote $(n_K + 3) \times 1$, $(n_n + 3) \times 1$ and $(n_K + 3) \times (n_n + 3)$ matrices respectively.

$$s(K, n) = [u_{j_K}(K)]^T C_{j_K j_n} [u_{j_n}(n)] \tag{A.19}$$

where $j_K = 1, \ldots, n_K + 3$ and $j_n = 1, \ldots, n_n + 3$

*Non-equidistant nodes*: For non-equidistant nodes similar approach used for equidistant nodes could be applied, if the nodes are mapped by re-scaling approach using certain grid function. This grid function maps the non-equidistant nodes by a strictly monotone, continuous one-to-one function to structure an equidistant grid.

## References

Asnafi, N., 1999. Analytical modeling of tube hydroforming. Thin-Walled Structures 34, 295–330.
Behforooz, G.H., Papamichael, N., 1979. End conditions for cubic spline interpolation. IMA Journal of Applied Mathematics 23, 355–366.
De Boor, C., 2001. A Practical Guide to Splines, revised edition Springer Publication, New York.
Dohmann, F., Hartl, Ch., 1997. Tube hydroforming – research and practical application. Journal of Materials Processing Technology 71, 174–183.
Gelin, J.C., Labergere, C., 2002. Application of optimal design and control strategies to the forming of thin walled metallic components. Journal of Materials Processing Technology 125–126, 565–572.
Habermann, C., Kindermann, F., 2007. Multidimensional spline interpolation – theory and applications. Computational Economics 30, 153–169.
Koc, M., Altan, T., 2001. An overall review of the tube hydroforming (THF) technology. Journal of Materials Processing Technology 108, 384–393.
Lin, F.C., Kwan, C.T., 2004. Application of abductive network and FEM to predict an acceptable product on T-shape tube hydroforming process. Computers & Structures 82, 1189–1200.
Nordlund, P., 1998. Adaptivity and wrinkle indication in sheet-metal forming. Computational Methods in Applied Mechanical Engineering 161, 127–143.
Ray, P., Mac Donald, B.J., 2004. Determination of the optimum load path for tube hydroforming processes using a fuzzy load control algorithm and finite element analysis. Finite Elements in Analysis and Design 41, 173–192.
Strano, M., Jirathearanat, S., Shr, S., Altan, T., 2004. Virtual process development in tube hydroforming. Journal of Materials Processing Technology 146, 130–136.
Xia, Z.C., 2001. Failure analysis of tubular hydroforming. Journal of Engineering Materials and Technology 123, 423–429.

Please cite this article in press as: Ghosh, A., et al., Database for real-time loading path prediction for tube hydroforming using multidimensional cubic spline interpolation. J. Mater. Process. Tech. (2010), doi:10.1016/j.jmatprotec.2010.09.012